

Wind farm control for wake-loss compensation, thrust balancing and load-limiting of turbines

Gonzalez Silva, Jean; Ferrari, Riccardo; van Wingerden, Jan Willem

DOI

[10.1016/j.renene.2022.11.113](https://doi.org/10.1016/j.renene.2022.11.113)

Publication date

2023

Document Version

Final published version

Published in

Renewable Energy

Citation (APA)

Gonzalez Silva, J., Ferrari, R., & van Wingerden, J. W. (2023). Wind farm control for wake-loss compensation, thrust balancing and load-limiting of turbines. *Renewable Energy*, 203, 421-433. <https://doi.org/10.1016/j.renene.2022.11.113>

Important note

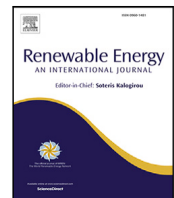
To cite this publication, please use the final published version (if applicable). Please check the document version above.

Copyright

Other than for strictly personal use, it is not permitted to download, forward or distribute the text or part of it, without the consent of the author(s) and/or copyright holder(s), unless the work is under an open content license such as Creative Commons.

Takedown policy

Please contact us and provide details if you believe this document breaches copyrights. We will remove access to the work immediately and investigate your claim.



Wind farm control for wake-loss compensation, thrust balancing and load-limiting of turbines

Jean Gonzalez Silva^{*}, Riccardo Ferrari, Jan-Willem van Wingerden

Delft University of Technology, Delft Center of Systems and Control, Delft, 2628CD, The Netherlands

ARTICLE INFO

Keywords:

Active power control
Thrust balance
Wake effects
Reliability
Integral control
Wind farm control

ABSTRACT

As renewable energy sources such as wind farms become dominant, new challenges emerge for operating and controlling them. Traditionally, wind farm control aims to dispatch power set-points to individual turbines to maximize energy extraction and, thus, their usage as assets. Yet, grid balance and frequency support are fundamental in presence of high renewable penetration and volatility of energy prices and demand. This requires a paradigm change, moving from power maximization to revenue maximization. In this paper, three active power control strategies pushing this shift of paradigm are investigated, namely: wake-loss compensation, thrust balancing, and load-limiting control.

The findings of large eddy simulations of a reference wind farm show that wake-loss compensation indeed improves the power generation on waked wind farms, but at the price of increased structural loads on certain turbines. The addition of a thrust balancing can equalize the stresses of individual turbines and their wear in the long term, while still attaining the required power output at the farm level. Furthermore, load-limiting controllers could potentially aid by allowing maintenance to be scheduled in a single time window, thus reducing operation and maintenance costs.

1. Introduction

According to the Global Wind Energy Council, 93.6 GW of new wind power was installed in 2021, which accounts for a 12.5% growth compared to 2020 [1]. Still, to meet the ambitious global plans for decarbonization, a growth of 180 GW per year would be required. The integration of wind power into the grid is becoming more relevant than ever as additional wind power capacity is commissioned each year across the globe. Future wind power plants will need to provide operational characteristics similar to those of conventional power plants, that comply with stricter grid code requirements and provide ancillary services to ensure safe and reliable operation of the power system [2,3]. As an example for other countries, the United Kingdom has laid out its “Net-zero” plan for 2050, which aims to increase offshore wind energy from around 7 GW today to 75 GW by 2050. Note that the peak demand for the United Kingdom in 2020 was about 48.76 GW [4]. Such a substantial increase in the volume of wind energy connected to the grid will require that wind farms no longer operate in a “greedy” manner, whereby the wind farms aim at maximizing energy capture. In addition, a drawback of the current concept of maximum power generation is the variance of aerodynamic loading across a dense farm due to the turbine interactions. Therefore, it is likely that wind farms will be required to participate in a more meaningful manner in the

grid balance, and consider the impact of their strategy on the structural loading of individual turbines.

Rapid penetration of renewable energy sources, with their inherently fluctuating energy availability, is still challenging for electric power systems. This raises questions about how the systems would operate when renewable generation becomes the dominant technology. The wind availability further reduces with farm densification due to turbine interactions, leading to overplanting as a trivial solution. In *overplanting*, the wind farm is conservatively designed and is expected to operate in derated conditions [5,6]. Balancing the wind farm production with the demanded grid loads can be provided by the so-called *Active Power Control* (APC), as demonstrated by Fleming et al. [7] in high-fidelity simulations. A centralized APC was introduced by an author [8], where a closed-loop controller is proposed to mitigate the oscillations of power generation caused by the wake effects, mainly the induced turbulence.

The ability to control the individual power output may lead to improvements in the provision of ancillary services [9–11]. The potential to regulate the active power, such as secondary frequency regulation, has relevant economic implications for wind farm operators [12]. As a result, turbines that directly participate in the system frequency stability significantly enhance their cost-effectiveness by eliminating

^{*} Corresponding author.

E-mail address: J.GonzalezSilva@tudelft.nl (J.G. Silva).

support mechanisms and improving the integration grid system. In addition, turbines under a power tracking controller, which does not operate to extract the maximum amount of power, are subjected to lower aerodynamic loads compared to those regulated by traditional controllers. This can lead to the extension of their service life [13–15]. Recently, new regulations have been pushing the wind industry towards the development of such technologies, with the Irish and the British grid codes being the first examples of the participation of wind power plants in frequency control [16,17]. These regulations require the provision of frequency control services directly from the wind turbines. Future trends for European regulations, like the European Network Code developed by the ENTSO-E, indicate the need for down-regulated wind turbines to participate in primary frequency control [18]. In literature, APC has been widely used for single wind turbines, where examples of wind turbine APC algorithms can be found in Aho et al. [19], Zhu et al. [20], Lio et al. [21], and Kim et al. [22]. Still, APC results are less explored in a wind power plant context where realistic flow interactions should also be taken into account.

While providing the required power output, wind farm control can be leveraged to reduce turbine loads [23,24]. As a strong driver of fatigue loading, wakes are known to induce turbulence due to both wake meandering and wake-added turbulence [25]. Reducing wake effects on downstream turbines could alleviate fatigue damage, especially on the blades. Recent research in this area can be found in [26–29]. In Vali et al. [27], tower base fore–aft bending moments are balanced while the wind farm power production follows a reference signal evaluated in a mid-fidelity model. In Stock et al. [29], the wind farm control dispatches power commands aiming to favor the loads in the turbines. A joint pitch-based and yaw-based control based on optimization algorithms is investigated by Kanev et al. [26] and, finally, the work in Baros et al. [28] implements a decentralized load control, where turbines can communicate with neighboring ones. All the above-mentioned works are either based on mid-fidelity simulations or real-time optimization algorithms whose computational costs are still high for practical implementation. These notions lead to a shifting paradigm whereby wind farm control can support better asset management under time-varying demand and electricity prices [30,31]. In the zero-subsidy era, maximizing revenue is likely to be prioritized over annual energy production gains. This can be achieved by reducing the active power production during periods of low grid loads demand and low electricity prices, as well as the optimization of loads for potential extension of the service life.

Recently, at an individual turbine level, condition-based control making use of down-regulation has become the focus of several publications, where turbines are down-regulated to reduce loading on specific components [14,15,32,33]. These strategies in the offshore environment are of great value since accessibility is the major barrier to offshore wind implementation. Long down periods and expensive maintenance events as results of faults are more prone to happen due to the harsh offshore environment, which includes wave loads and accelerated corrosion [34]. As an alternative to shutdown, down-regulation can have a significant cost-effective impact on production by safely operating damaged turbines [35]. Turbine operations can be constrained to provide more structural reliability by being self-aware of possible non-designed conditions [36,37]. Also, the Levelized cost of electricity can be reduced by avoiding unexpected maintenance costs with preventive methods in long term.

The main contribution of this paper is the extended evaluation of three APC strategies for wind farm control, namely wake-loss compensation, thrust balancing, and load-limiting control. This evaluation is conducted in terms of power generation and mechanical loads across the entire wind farm. First, the active power compensation of wake losses uses the current turbine power output to enhance the tracking of defined power demand. Therefore, the power system's reliability is increased by maintaining the electrical frequency close to nominal. Second, a thrust balancer uses estimations of aerodynamic forces to

equalize thrust forces in all possible turbines in the farm depending on their wind power availability. This leads to a uniform distribution of structural loads across the turbines. As consequence, the degradation of high-loaded turbines is reduced together with their associated maintenance costs. In addition, the total farm available power can be increased by the cooperative farm operation, as seen in [38]. Lastly, a load-limiting strategy using the instantaneous thrust estimations derived from regular turbine measurements, i.e. rotor speed, generator torque, and blade pitch angles, switches its feedback loop between tracking the power reference signal and limiting the instantaneous thrust force based on a user-defined thrust force threshold. As a prevention measure of structural faults, the threshold should be defined by the operator or health monitoring systems due to unexpected or accumulated damage to the turbine structure. This load-limiting strategy based on a power tracking controller is explored at the wind farm level in contrast to the existing literature.

A reference wind farm layout is simulated in a high-fidelity environment. Results compare the APC strategies in terms of root mean squared, mean absolute, and peak errors; as well as, time-averaged means, standard deviations, and damage-equivalent loads. The damage-equivalent loads are computed for the turbine rotor shaft, tower base, and blade root. The findings show that the proposed wake-loss compensation exhibits a simple and effective concept that significantly improves wind farm power tracking in waked conditions. As the wake-loss compensation does not consider wake models for simplicity, the variance of loads is an undesirable side effect. Then, the aerodynamic loads are balanced by the thrust balancer, as well as the standard deviations of damages in distinct turbine components are reduced. This effectively mitigates the variance of loads on the farm. Furthermore, specific turbines have their structural damages drastically reduced using the load-limiting control based on the instantaneous load estimations while the effects on the wind farm power generation are minor.

The structure of this paper is as follows. First, the simulation environment is defined in Section 2. Next, Section 3 thoroughly describes the working principles of the proposed control approaches. The potential of these approaches as a future trend in wind farm control will then be demonstrated in Section 4 through high-fidelity simulations. Finally, the paper is concluded in Section 5.

2. Simulation environment

The proposed control strategies are evaluated in the Simulator for Wind Farm Applications (SOWFA) [39]. SOWFA is a high-fidelity large-eddy simulation (LES) tool developed at the National Renewable Energy Laboratory (NREL). The flow is simulated using OpenFOAM [40] by solving the three-dimensional unsteady Navier–Stokes equations and transport of potential temperature equations, which take into account the thermal buoyancy and earth rotation (Coriolis) effects in the atmosphere over a discretized domain. SOWFA couples the OpenFOAM CFD solver with NREL's OpenFAST wind turbine simulator [41]. Realistic ambient atmospheric turbulence intensity, determined by inflow turbulence and the atmospheric thermal stability conditions, is created using precursor simulations. The wind turbines are modeled using a rotating actuator disk model (ADM-R) [42].

Previous studies have been performed to validate SOWFA. For example, SOWFA has been compared with the 48-turbine Lillgrund wind plant field data and shows good agreement through the first five turbines in a row aligned with the wind direction [43]. In addition, SOWFA has been tested to verify that the inertial range in the turbulent energy spectra and the log-profile in the mean flow are incorporated, both of which characterize a realistic atmospheric boundary layer [44].

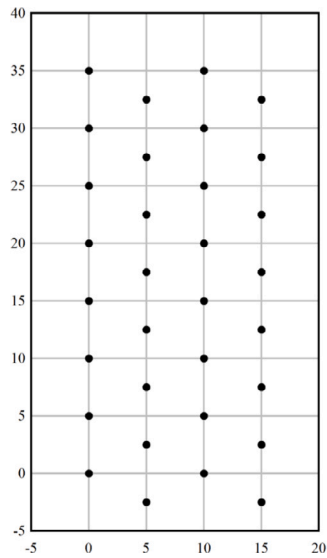


Fig. 1. Layout of the TotalControl reference wind power plant. Units of axes are rotor diameters [45].

2.1. Wind farm layout

The TotalControl reference wind power plant (TC-RWPP) defined in the H2020 TotalControl project is a virtual test bed for wind farm control [45]. The TC-RWPP is a suitable reference wind farm for simulating moderate and high waked conditions depending on different inflow orientations. Fig. 1 shows the staggered pattern of the TC-RWPP composed of 32 wind turbines. The separation between rows and columns is five rotor diameters ($5D$). This layout assumes that the prevailing wind direction is from the west in Fig. 1. In this low wake interaction scenario, the wakes of upstream turbines hit a single turbine in the stream. In this work, we also explore a medium wake interaction scenario, where four-turbines wake interactions occur. The latter happens when the wind direction deviates 26.565° from the first scenario.

The yaw control, often implemented in a decoupled control loop, aims to align the turbine nacelle with the wind direction. Using a low-pass filtered wind direction signal from wind sensors (nacelle anemometers and/or wind vanes), a yaw angle or yaw rate is commanded to the yaw actuator to assure optimal inflow conditions. The simulations were executed with constant wind directions aiming full-waked conditions. The full-waked conditions present larger effective wind speed deficits between turbines, consequently bigger power tracking errors. Partial-waked conditions or time-varying wind directions are supposed to be easier handled by the controllers and are not the focus herein.

The simulated turbines are DTU 10 MW Reference Wind Turbines [46], which have rotor diameter of $D = 178.3$ m. The inflow wind direction in the simulator is from the southwest (240°), instead of the assumed prevailing wind direction from the west (270°). This is done to generate appropriate turbulent wind conditions by precursor simulations. Details about the positioning of the turbines in the domain for each scenario are depicted in Figs. 2 and 3, where the layout is accordingly rotated -30° and -3.435° , respectively.

The distance between interacting turbines is different between the two studied scenarios. In the first scenario, the distance between the free-stream turbines and the turbines under the wake is $10.0D$, with sixteen interactions between two turbines. In the second scenario, the distance is about $5.59D$ and there are two turbines in the free stream that are not affecting the downstream turbines, two sets of three turbines, and six sets of four turbines under wake interaction.

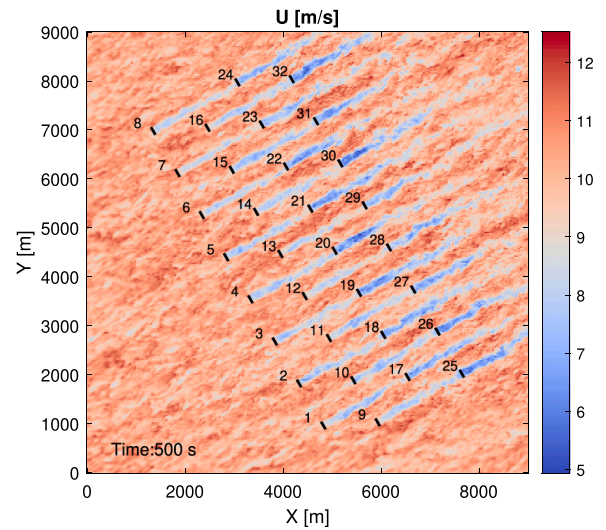


Fig. 2. Layout of the simulated 8-by-4 wind farm rotated by -30° for the low wake interaction scenario. The background is an instantaneous horizontal slice of flow output taken from a Simulator for Wind Farm Application (SOWFA).

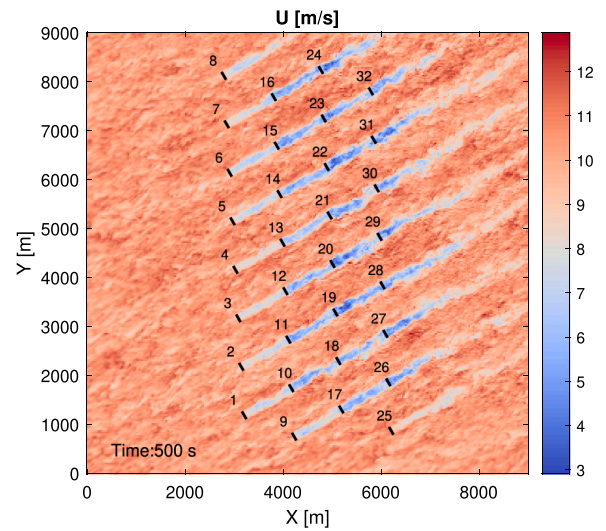


Fig. 3. Layout of the simulated 8-by-4 wind farm rotated by -3.435° for the medium wake interaction scenario. The background is an instantaneous horizontal slice of flow output taken from a Simulator for Wind Farm Application (SOWFA).

2.2. Simulation parameters

The simulation parameters are summarized in Table 1. The spatial discretization mesh for CFD is one-step refined in a rectangular region, where the turbines are located and wakes are developed. Above 300 m of height, the mesh is coarser to reduce computation time.

In all cases, the conditions simulated in SOWFA are based on the study by Churchfield et al. [44]. The simulated atmospheric conditions consist of a neutral atmospheric boundary layer with a low aerodynamic surface roughness value of 0.002 m — typically for offshore sites. The wind speed intensity averages 10 ms^{-1} and the turbulence intensity is around $5\text{--}6\%$ at the turbine hub height. The simulated time length of 1000 s is used to let the wakes develop through the domain. We were limited by single simulations for each controller approach because of the associated enormous computational cost due to the large simulated domain. Yet, the exact same turbulent inflow field is used.

A power tracking controller, further presented in Section 3.1, can follow a time-varying automatic generation control (AGC) signal. The

Table 1
SOWFA simulation parameters.

Property	Value
Domain size	9 km × 9 km × 1 km
Cell size outer region	10 m × 10 m × 10 m
Cell size near rotors	5 m × 5 m × 5 m
Simulation time-step	0.5 s
Atmospheric boundary layer (ABL) stability	Neutral
Mean inflow wind speed	10 m/s
Surface roughness	0.0002 m
Turbulence intensity	5.0-6.0%
Turbine rotor approximation	Rotational Actuator Disk Model (ADM-R) [42]
Turbine type	DTU 10 MW [46]
Turbine rotor diameter	178.3 m
Turbine hub height	119 m
Force scalar factor	1.0
Inflow velocity factor	0.94
Blade smearing factor	20.0 m
Inter-turbine interaction spacing	10.0 D and 5.59 D^3

^aThe inter-turbine interaction spacing depends on the wind direction because of the staggered pattern defined in Section 2.1.

AGC command used here is a portion of the 40-minute ‘RegD’ test signal, the most rapidly actuating test signal that is used for AGC qualification by the PJM regional transmission organization [47]. The signal is normalized and upsampled to 1 Hz. In the simulations, we assume a power command to have a persistent value of 3.5 MW, lower than half of the maximum produced power at a wind speed of 10 ms⁻¹, plus an AGC perturbation signal, which is set to have an amplitude of 1 MW. The AGC signal starts at 300 s to allow time for the wakes to develop and propagate during the simulation.

3. Control strategies

3.1. Individual wind turbine control

In variable-speed, variable-pitch machines, the rotational speed, and the grid frequency are decoupled due to an indirect connection between generator and grid, which is carried out, nowadays, by the so-called back-to-back converters [48]. This concept is about 25 years old and allows wind turbines to down-regulate by reducing their speed while the grid frequency is maintained.

Herein, the wind turbine controller is synthesized to track a reference power signal whenever possible. Down-regulation based on blade pitch is considered. The controller shows a resemblance with the pitch-reserve controller described in Aho et al. [19] and the KNU2 algorithm in Kim et al. [22]. The choice based on blade pitch is justified by the following characteristics: a monotonic thrust reduction in response to monotonic demanded power reduction is achieved; operation close to the min- C_T method [20]; ensuring a stability margin w.r.t. stall regions [49].

The turbines are down-regulated by applying both the blade pitch and generator torque. The blade pitch controller consists of a gain-scheduled PI control law, where the blade pitch command θ is defined as

$$\theta = \frac{\bar{K}_P(\theta_{meas})}{s} [\omega_{gen, meas} - \omega_{gen, ref}(P_{dem})] + \frac{\bar{K}_I(\theta_{meas})}{s} [\omega_{gen, meas} - \omega_{gen, ref}(P_{dem})], \quad (1)$$

in which $\omega_{gen, meas}$ and θ_{meas} , respectively, are the measured generator speed and the measured collective blade pitch angle. The reference generator speed, $\omega_{gen, ref}$, is a function of the demanded power P_{dem} . $\bar{K}_P(\theta_{meas})$ and $\bar{K}_I(\theta_{meas})$ are the gain-scheduled proportional and integral gains [50].

The blade pitch controller, as a feedback loop, seeks to regulate the generator speed to the desired reference speed and it is similar to the

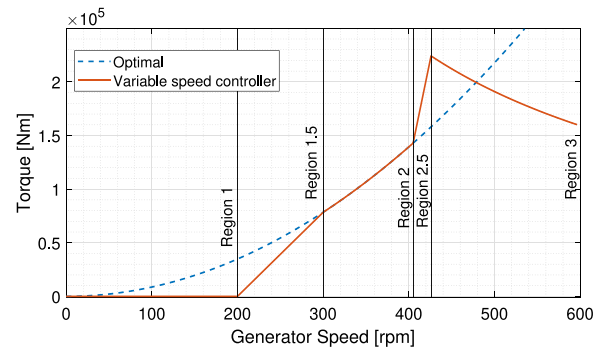


Fig. 4. Generator torque as a function of the rotor speed for the DTU 10MW Reference Wind Turbine.

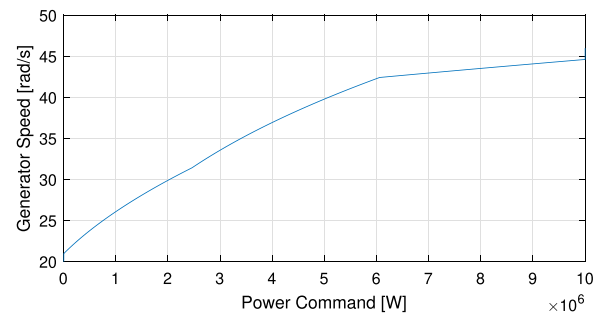


Fig. 5. Generator speed reference as a function of the demanded power for the DTU 10MW Reference Wind Turbine.

controller used for generator speed regulation in above-rated conditions, traditionally. However, the generator speed setpoint depends on the demanded power rather than a rated value, $\omega_{gen, rated}$, as depicted in Fig. 5. The relation in Fig. 5 is obtained by the traditional generator torque–speed curve from Fig. 4. The generator speed setpoint is selected by the same amount of power that the turbine would generate by *greedy control* in different wind conditions and it is upper-bounded by the rated value. The literature standard for wind turbine control is referred to as *greedy control*. The reader is referred to [51,52] for more information on *greedy control* and [50,53] for practical implementation of such a controller.

Together with the blade pitch controller, the generator torque controller is usually applied to track the demanded power by multiplying it by the inverse of the measured generator speed as

$$\tau_{gen, tracking} = \frac{P_{dem}}{\eta_{eff} \omega_{gen, meas}}, \quad (2)$$

where η_{eff} is the generator efficiency. This controller would provide near-perfect tracking by meeting the generated with the demanded power. However, this generator torque control law can be problematic as a certain increase in demanded power might lead to undesirable lower rotor speed and shut-off. In the *greedy control*, the generator torque is known to be stable for $\omega_{gen} \geq 0$, and globally converges to the optimal power coefficient C_p to maximize the turbine’s power production (in region 2). The greedy torque control law,¹ which is composed of the traditional regions, is represented by $\tau_{gen, greedy}$ and depicted in Fig. 4. Therefore, combining the greedy torque with the power tracking control law yields

$$\tau_{gen, combined} = \min(\tau_{gen, greedy}, \tau_{gen, tracking}). \quad (3)$$

¹ In the industry, the optimal torque law in region 2 is often replaced with a PID-controller-based tip-speed-ratio tracking algorithm in combination with a wind speed estimator. Such an algorithm does not sufficiently add to the relevance of this work and therefore is outside the scope of this paper.

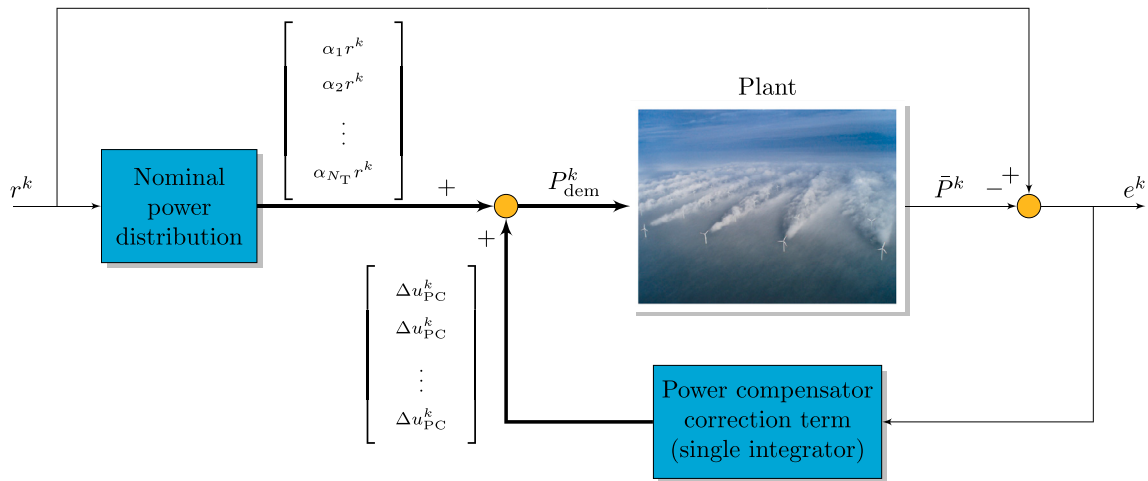


Fig. 6. Block diagram of the wake-loss compensator.

The generator torque control law in Eq. (3) ensures that the turbine does not operate at a lower tip-speed ratio than expected due to fast transients. As a result, imminent shutdowns are prevented and the turbine operates conservatively avoiding stall. Near-perfect power tracking is achieved whenever $\tau_{gen, tracking}$ is not constrained by $\tau_{gen, greedy}$ and $P_{dem} \leq P_{greedy}$, where P_{greedy} is the hypothetical power produced by greedy control with the current wind inflow. At low available power in the wind, the turbine controller completely switches to *greedy control* whenever the collective blade pitch angle reaches the switch value θ_{switch} , and the generator speed becomes lower than the reference speed. This keeps the turbine producing the maximum power while it is saturated.

The derived power tracking controller at individual turbine level is extended to the control of the wind farm in the following subsections, as in [54].

3.2. Wind farm control: wake-loss compensation

Whenever a wind farm rather than the individual wind turbines are to track a reference power signal, the power setpoint distribution over the turbines must be decided on. The power that a turbine can produce is directly correlated to the local wind speed and varies within the farm due to wake interactions. This leads to a non-trivial problem of distributing a wind-farm-wide power reference signal over individual turbines. In this subsection, a model-free and closed-loop controller is synthesized to distribute the power setpoints among the turbines and to minimize the wind-farm-wide reference tracking error as shown in Fig. 6.

The input signal of a single turbine is the demanded power P_{dem} , and the actual power produced P_{gen} is its output. In the situation that the turbine saturation does not occur, i.e. $P_{dem} < P_{greedy}$, and at near-perfect tracking, the input–output relationship is

$$P_{gen}^k = \tau_{gen, tracking}^k \omega_{gen}^k \eta_{eff} = P_{dem}^{k-1} (\omega_{gen, meas}^{k-1} \eta_{eff})^{-1} \omega_{gen}^k \eta_{eff}, \quad (4)$$

where k is the discrete-time index of the simulation and controller. With a sufficiently high sampling rate about 1–10 Hz, we can assume $\omega_{gen}^k \approx \omega_{gen, meas}^{k-1}$ and therefore, $P_{gen}^k \approx P_{dem}^{k-1}$. Thus, the wind turbines can be approximated as pure time-delay systems² with their time delay equal to the simulation sampling time Δt , where the time $t^k = t^{k-1} + \Delta t$. Now, consider power track at the farm scale. The wind-farm-wide power

² Pure time-delay systems have their response delayed by a time period. Time-delay systems inherently limit controller design due to right-half-plane zero (nonminimum-phase) behavior.

reference $r^k \in \mathbb{R}$ is to be divided among the turbines. Mathematically, the demanded power signal $P_{dem, i}^k \in \mathbb{R}$ for each turbine i is

$$P_{dem, i}^k = \alpha_i r^k + \Delta u_{PC}^k, \quad \text{with} \quad \sum_{i=1}^{N_T} \alpha_i = 1. \quad (5)$$

The term α_i divides the total wind farm power over the N_T turbines, defined as the nominal active power distribution, here assumed to be time-invariant and uniform for simplicity, i.e. $\alpha_i = \alpha_j, \forall i, j$. Still the target of further research, a smart nominal power distribution would benefit the operation of turbines. The global correction term $\Delta u_{PC}^k \in \mathbb{R}$, as in van Wingerden et al. [8], is the output of a pure integral controller defined as

$$u_{PC}^k = u_{PC}^{k-1} + K_{I, PC} e^k \Delta t, \quad \text{with} \quad e^k = r^k - \bar{P}^k, \quad (6)$$

where $K_{I, PC}$ is the integrator gain for the power compensator. The pure integrator controller is designed to compensate for the instantaneous wind-farm-wide tracking error e^k , which is obtained from the wind-farm-wide reference r^k to the sum of all individual active power production $\bar{P}^k \in \mathbb{R}$. Although the proportional action might lead to faster responses, it is not included because turbine saturation can lead to undesirable aggressive behaviors, as well as the simplicity of the proposed control design can be kept. The integrator gain is chosen as $K_I = N_T^{-1} \Delta t^{-1}$, which is by definition the optimal controller for time-delay systems without turbine saturation.³ The error e^k would therefore be eliminated on the next time-step, whenever all turbines are not saturated.

Using the integrator, the wind farm power tracking stability is assured, where the accumulated error tends to be eliminated in a steady state. Integrator anti-windup is implemented when all turbines are saturated. Moreover, the integrator state resets whenever all turbines are not saturated. This controller should achieve near-perfect tracking limited by the time delay and overall power availability.

3.3. Wind farm control: thrust force balancing

The thrust force balancer is developed to reduce high thrust forces encountered inside the farm due to wake effects. The thrust forces, considered as the mean of the aerodynamic loads in the rotor, are reduced in these turbines, consequently, reducing their fatigue. Reducing

³ Gain-scheduling due to turbine saturation are not considered and increases undesirable significant transients. Therefore, whenever saturation occurs, the wind farm control operates sub-optimally but with smother transients.

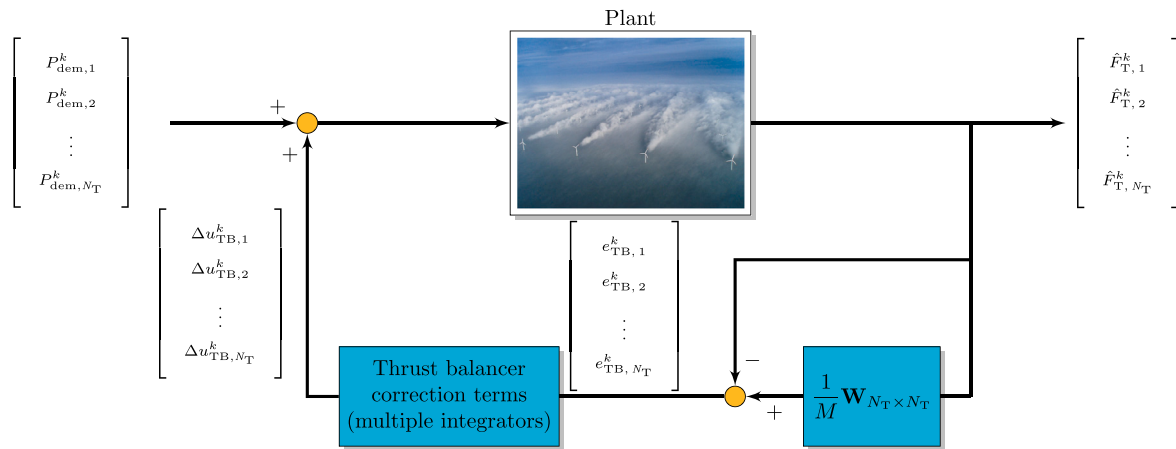


Fig. 7. Block diagram of the thrust balancer.

the variation of thrust forces across the farm extends the aggregated turbine life. The main idea of the thrust force balance controller is to balance the thrust forces of all turbines to their mean value while the wind farm power tracking is maintained [38]. Hence, in addition to the power compensator feedback, a thrust control loop is synthesized by using each of the estimated instantaneous thrust forces $\hat{F}_{T,i}^k$. At each step-time, all $\hat{F}_{T,i}^k \in \mathbb{R}$ are subtracted by their mean thrust force $\bar{F}_T^k \in \mathbb{R}$ to obtain the thrust force error vector $e_{TB}^k \in \mathbb{R}^{N_T}$.

In the control development, we noticed that the additional loop, depicted in Fig. 7, would unsuccessfully try to boost the generated power of saturated turbines. In addition, the loop would reduce the demanded power of the unsaturated turbines which might be used for compensation purposes. Consequently, both loops compete with each other. Therefore, to make sure that the feedback loops will not compete, turbines that are saturated, which usually have lower thrust forces, are removed from the mean thrust force computation through the balance weight matrix

$$\mathbf{W}_{N_T \times N_T} = \begin{bmatrix} s_1 & s_2 & \dots & s_{N_T} \\ s_1 & s_2 & \dots & s_{N_T} \\ \vdots & \vdots & \ddots & \vdots \\ s_1 & s_2 & \dots & s_{N_T} \end{bmatrix}, \text{ where } \begin{cases} s_i = 1, & \text{if turbine is} \\ & \text{not saturated;} \\ s_i = 0, & \text{if turbine is} \\ & \text{saturated.} \end{cases} \quad (7)$$

Also, the corresponding instantaneous thrust force errors of saturated turbines are reset as

$$e_{TB,i}^k = 0, \text{ if turbine is saturated.} \quad (8)$$

Then, the instantaneous thrust force error vector, e_{TB}^k , is computed as

$$e_{TB}^k = \left(\frac{1}{M} \mathbf{W}_{N_T \times N_T} - \mathbf{I} \right) \hat{\mathbf{F}}_T^k, \quad (9)$$

in which M is the number of turbines that are not yet saturated, \mathbf{I} the identity matrix, and $\hat{\mathbf{F}}_T^k \in \mathbb{R}^{N_T}$ the vector containing all of the estimated instantaneous thrust forces. Analogous to the wake-loss compensation, pure integral controllers are designed to eliminate the individual instantaneous thrust force errors with respect to the overall mean of the unsaturated turbines, as

$$u_{TB,i}^k = u_{TB,i}^{k-1} + K_{I,TB} e_{TB,i}^k \Delta t, \quad (10)$$

where $K_{I,TB}$ is the integrator gain for the thrust balancing, chosen to be the same value for the multiple integrators. The tuning procedure relies on the identification of the model dynamics from the demanded power to the thrust force of the defined down-regulator in Section 3.1. For brevity, the reader is referred to [38] for more details. Finally, the corresponding correction terms in $\Delta u_{TB}^k \in \mathbb{R}^{N_T}$ are added to demanded powers $P_{dem}^k \in \mathbb{R}^{N_T}$ to balance all thrust forces of unsaturated turbines.

3.3.1. Thrust estimation

The estimated instantaneous thrust force \hat{F}_T , which represents the main aerodynamic load, is obtained from the steady state model and the regular turbine measurements as

$$\hat{F}_T = 0.5 \rho \pi R^2 \hat{v}_w^2 C_T \left(\frac{R \omega_{r,meas}}{\hat{v}_w}, \theta_{meas} \right), \quad (11)$$

in which \hat{v}_w is the estimated effective wind speed [55], ρ the air density, R the rotor radius and C_T the thrust coefficient from pre-computed mapping with the measured rotor speed $\omega_{r,meas}$ and collective blade pitch angle θ_{meas} . In this work, the estimation of the effective wind speed is obtained from an I&I estimator [56] through measurements of rotor speed, generator torque, and blade pitch angles. Note that \hat{F}_T is therefore a mean of the inflow loads over the rotor, where the inflow is inherently not constant by shear, wake, and other effects.

3.4. Wind turbine control: load-limiting control

For damaged turbines, the balance of thrust force might not be enough to guarantee safety. Such turbines require lower instantaneous loads to keep high safety levels/factors. Lastly, health monitoring systems are increasingly becoming a feasible technology for wind turbines [57,58]. Therefore, the operation of those turbines should be appropriately constrained in real-time by the controller while still producing energy.

The down-regulation method in Section 3.1 reduces the structural stresses when reducing power demand. Thus, the turbine would be able to continue operating by down-regulating accordingly with the current loads as opposed to shutting down, until maintenance is fully performed. Although this results in sub-optimal power generation in the damaged turbines, the turbines' structural reliability is improved, where fatigue damage is alleviated and lifetime extended [35]. Also, as seen in Section 3.2, the power contributions from individual turbines can be redistributed among the turbines in the farm. That is, reducing the demanded power for a set of turbines can be compensated for by increasing the power generation in other turbines.

A switching control architecture for individual turbines, depicted in Fig. 8, is therefore implemented in a wind farm setting. A user-defined constraint on the instantaneous thrust force is to be satisfied while the reduction in power generation is compensated by the other turbines. In the defined turbine j , the architecture allows for a demanded power profile to be tracked when the thrust force is lower than a given maximum allowed value $\bar{F}_{T,j}$. When such a value is reached, the proposed controller switches from tracking the demanded power to tracking the maximum allowed thrust force through feedback, thus satisfying the constraint on the maximum turbine instantaneous load.

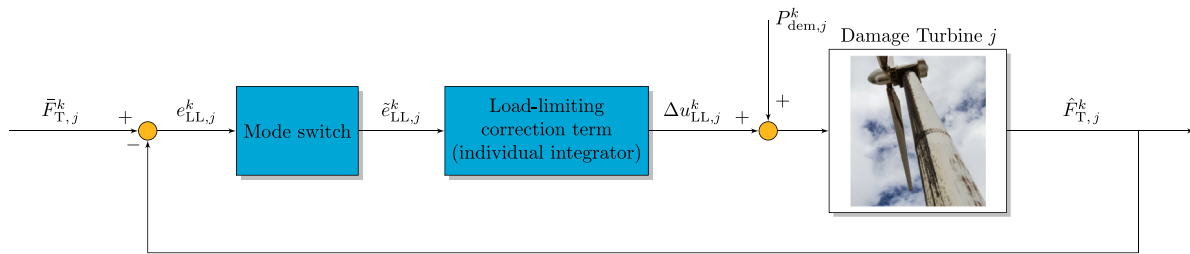


Fig. 8. Block diagram of the load-limiting control.

The first observation is that, in order to not modify the power demand reference signal, it is sufficient for the additional local signal $\Delta u_{LL,j} \in \mathbb{R}$ to become zero. In order to do this, a Mode Switch is designed such that the new additional local feedback loop will be open whenever the constraint on the thrust force is not exceeded. In particular, the switching will be defined by introducing the following signal

$$\tilde{e}_{LL,j} = \begin{cases} e_{LL,j}, & \text{if } e_{LL,j} < 0 \text{ or } e_{LL,1,j} < 0 \\ 0, & \text{otherwise} \end{cases} \quad (12)$$

where $e_{LL,j}^k = \bar{F}_{T,j}^k - \hat{F}_{T,j}^k$ and $e_{LL,1,j}^k = \int_0^{k\Delta t} e_{LL,j}(\tau) d\tau$ represent, the difference between the estimated instantaneous thrust force and its upper bound, and the time integral thereof. The rationale for this definition with the inclusion of the integral term is to avoid *chattering* when the thrust force is close to its reference, as is done for instance in the literature on Integral Sliding Mode control [59].

When the mode switch is active – that is when $\tilde{e}_{LL,j}^k \neq 0$ – the local feedback loop is closed. Using a simple pure integrator, as in previous subsections, the local correction signal $\Delta u_{LL,j}^k \in \mathbb{R}$ is obtained by

$$u_{LL,j}^k = u_{LL,j}^{k-1} + K_{I,LL} \tilde{e}_{LL,j}^k \Delta t, \quad (13)$$

where $K_{I,LL}$ is the integrator gain for the load-limiting loop. For further details, see [36]. As the load-limiting controller directly makes use of down-regulation, its stability is guaranteed by the down-regulation method — Section 3.1; i.e. if the down-regulation method is stable to demanded power changes, so is the controller using an integrator. This extends to all methodologies in this work. The parameters used in the simulations are presented in Table 2.

4. Results

The key findings in this paper are illustrated via a series of event plots and tables in this section, focusing on generated and reference power signals, turbine actuation, and mechanical loads. The results are obtained by the cumulative use of the defined controllers in Section 3. One of the differentiating features of this work is the analysis of full farm signals and loads. Thus, the results are broken down by quantities of interest, which encompass turbine operational parameters, such as blade pitch and generator torque, and key structural loads, including out-of-plane blade root bending moment, shaft torque, and tower-base bending moment. Time-domain histories of the quantities of interest are presented via aggregate statistics, in particular mean values, standard deviations, root mean squared errors, mean absolute errors, peak errors, and short-term damage equivalent loads (DELs).

4.1. Statistical calculations

Root mean squared error (RMSE) is considered an excellent general-purpose error metric for tracking performance, as it is scale-dependent.

$$RMSE = \sqrt{\frac{1}{N} \sum_{n=1}^N |x_n - x_n^{ref}|^2}, \quad (14)$$

where N is length of the evaluated discrete signal x , n the element variable, and x^{ref} the reference signal.

Mean absolute error (MAE), as also a widely used criterion, is defined by

$$MAE = \frac{1}{N} \sum_{n=1}^N |x_n - x_n^{ref}|. \quad (15)$$

This criterion is a similar measurement to the RMSE. Nevertheless, it is more robust since it is less sensitive to extreme values than RMSE. In MAE, different errors are not weighted, but the scores increase linearly with the increase in errors. Generally speaking, low values for RMSE and MAE mean that the power generation has been accurately tracking the power reference.

Moreover, peak error (PE) is defined by

$$PE = \max_{n \in \{1, \dots, N\}} |x_n - x_n^{ref}|. \quad (16)$$

Short-term fatigue DELs of quantities of interest were computed directly from the time series using the NREL postprocessing tool, MLife [60]. MLife uses rainflow counting to bin a histogram of load

Table 2
Parameters of controllers.

Variable	Symbol	Value
Proportional gain of the pitch controller	\bar{K}_p	Gain-scheduled; 0.039–1.41 s [50]
Integral gain of the pitch controller	\bar{K}_i	Gain-scheduled; 0.067–0.28 s [50]
Derivative gain of the pitch controller	\bar{K}_D	0.0 s [50]
Corner frequency of generator speed low-pass filter	–	0.1798 Hz [50]
Generator efficiency	η_{eff}	1 [50,53]
Generator torque constant for greedy control	K_{greedy}	79.43986 N m/(rad/s) ² [50]
Transitional generator speed bet 1.5 to 2	–	200.0 rpm [50]
Transitional generator speed — region 2 to 2.5	–	300.0 rpm [50]
Transitional generator speed — region 2 to 2.5	–	405.0 rpm [50]
Rated generator slip percentage in region 2.5	–	10.0 [52]
Rated power	P_{rated}	10 MW [46]
Transitional generator speed between regions 2.5 and 3 percent of rated generator speed	–	95.0 [52]
Rated generator speed	$\omega_{gen,rated}$	445.67 rpm [52]
Maximum generator rate	–	15,000 N m/s [50,53]
Maximum blade pitch rate	–	10 deg/s [50,53]
Fine blade pitch angle	θ_{fine}	0.75 deg [50]
Switch blade pitch angle	θ_{switch}	1 deg [50]
Integral gain of the wind farm wake-loss compensator	$K_{I,PC}$	$N_T^{-1} \Delta t^{-1a}$
Integral gain of the wind farm thrust balancer	$K_{I,TB}$	0.5 [38]
Integral gain of the wind turbine load-limiting controller	$K_{I,LL}$	2.947 [36]

^aOptimal gain defined in Section 3.2.

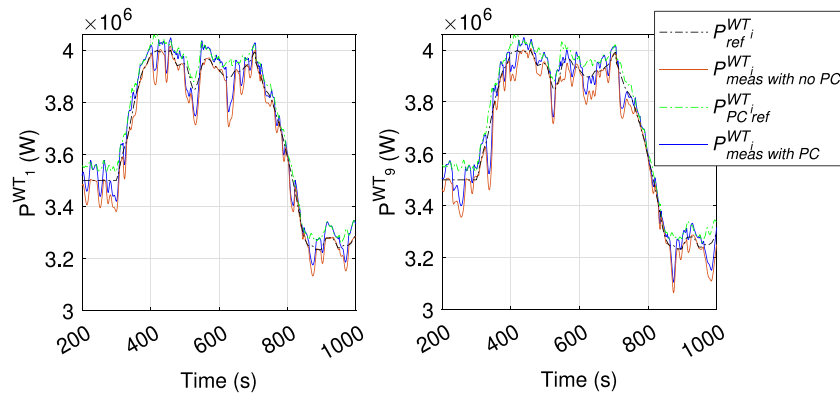


Fig. 9. Powers of turbine 1 and 17 in Scenario 1. $P_{ref}^{WT_i}$ is the uniform dispatch power of the desired wind farm power, $P_{meas}^{WT_i}$ the obtained power with no power compensation, $P_{PC\ ref}^{WT_i}$ the new power reference given by the power compensator, and $P_{meas}^{WT_i}$ with PC the obtained power with power compensation.

cycle amplitudes over the time series. A mean-value Goodman correction is also used for the histogram amplitudes. The short-term DELs are computed from the histogram bins and the material-specific Wöhler exponent, m , from classical S–N fatigue theory, as in Eq. (17). As is standard practice, $m = 5$ was used for loads on the main shaft and tower made of steel, and $m = 10$ for loads on the composite blades.

$$DEL_{short} = \left[\frac{1}{T} \sum_k c_k f_k^m \right]^{\frac{1}{m}}, \tag{17}$$

in which T is the simulation time representing a 1-Hz equivalent cycle, k is the number of bins, and c is the number of cycles at load amplitude, f .

4.2. Mechanical calculations

The computation of tower-base bending moment was simplified using only the component of the fore–aft thrust force F_T and the tower height h_t as

$$M_t = F_T h_t. \tag{18}$$

The ultimate tower-base bending moment is derived from the ultimate stress σ_{ult} of the tower material, considered as $\sigma_{ult} = 400$ MPa, and its geometry as

$$M_{t,ult} = \frac{\sigma_{ult} I_t}{r_{o,t}}, \tag{19}$$

in which I_t is the moment of inertia and $r_{o,t}$ is the outside radius of the tower base. The ultimate tower-base bending moment is considered $6.0 \cdot 10^5$ k m. Moreover, the ultimate shaft torque is derived considering pure torque loading, i.e. $\tau_{max} = \sigma_{ult}/2$, and shaft geometry as

$$T_{shaft,ult} = \frac{J_{shaft} \tau_{max}}{r_{o,shaft}}, \tag{20}$$

in which J_{shaft} is the polar moment of inertial and $r_{o,shaft}$ is the outside radius of the shaft. The ultimate shaft torque is therefore considered as $3.5 \cdot 10^6$ k m. Lastly, the out-of-plane root-blade bending moment is computed by summing the corresponding moments due to axial forces throughout the blade span. The ultimate blade root bending moment is considered $7.0 \cdot 10^4$ k m [46]. Note that, with a different definition from the Standards for Certification of wind turbines, the ultimate load is herein derived from each component for the computations of short-term fatigue DEL.

4.3. Simulations

The application of the active power control methodologies, namely wake-loss compensation, thrust force balancing, and load limitation

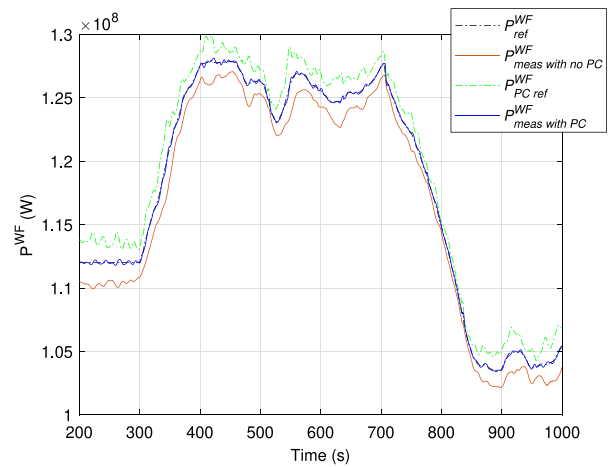


Fig. 10. The total wind farm power in Scenario 1. P_{ref}^{WF} is the desired power for the farm, P_{meas}^{WF} with no PC the obtained power with no power compensation, $P_{PC\ ref}^{WF}$ the new power reference from the power compensator, and P_{meas}^{WF} with PC the obtained power with power compensation.

was simulated in the low wake interaction scenario (Scenario 1) and the medium wake interaction scenario (Scenario 2). Moreover, the variability in wind energy is represented by a time-varying wind farm power reference signal, instead of varying wind conditions, as described in Section 2.

Wake-loss compensation. The closed-loop wake-loss compensator boost the individual wind turbine power references to compensate for power losses from wake effects. In Scenario 1, the power losses due to wake effects on downstream turbines are mild. The effects of oscillations due to the turbulence in the wind inflow are seen in the power output in Fig. 9. The power compensator, denoted as “PC”, slightly boosts the power reference signal to deal with them. Turbines 1 and 17, an upstream and a downstream turbine respectively, are plotted for the sake of brevity, as the other turbines in the farm behave similarly. The total wind farm power signals are presented in Fig. 10. The desired reference signal is depicted in black, the total power output signal without the proposed wake-loss compensator is in red, and the total power output signal when the PC is applied is in blue. Also, the total of the boosted power references signal in the PC simulation is plotted in green. Clearly, the PC as a wind farm closed-loop approach significantly enhances the total power trackability.

In Scenario 2, there are sets of three turbines under a consecutive full-waked flow and a lower inter-spacing distance, so the wake effects on the downstream turbines lead to a significant mismatch between

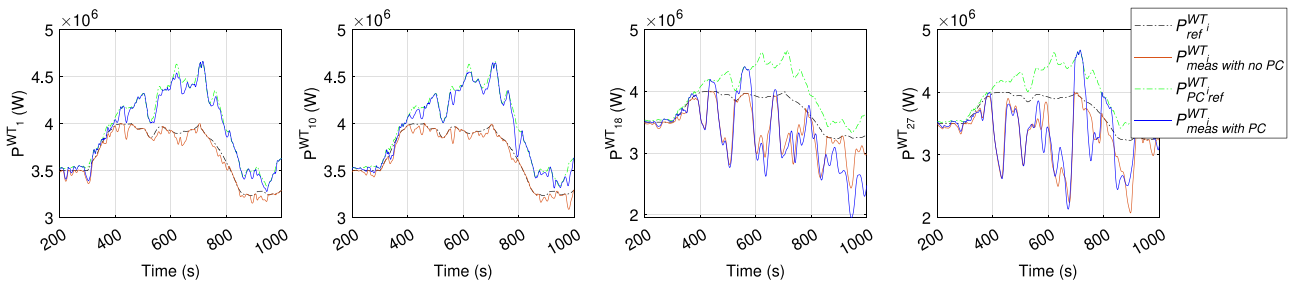


Fig. 11. Powers of turbines 1, 10, 18 and 27 in Scenario 2. $P_{ref}^{WT_i}$ are the uniform dispatch powers of the desired wind farm power, $P_{meas}^{WT_i}$ the obtained power with no power compensation, $P_{PC}^{WT_i}$ the new power reference from the power compensator, and $P_{meas}^{WT_i}$ the obtained power with power compensation.

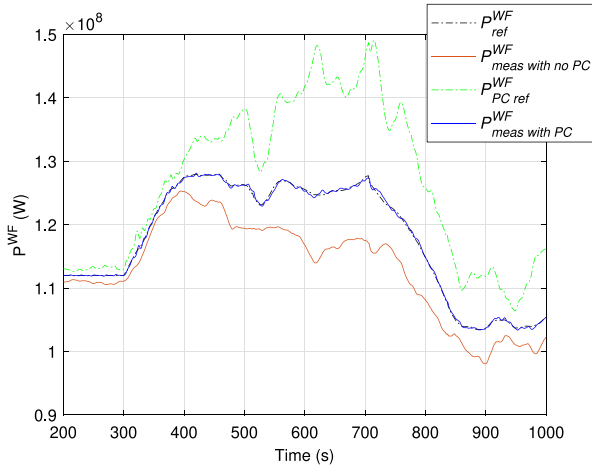


Fig. 12. The total wind farm power from Scenario 2. P_{ref}^{WF} is the desired power for the farm, P_{meas}^{WF} the obtained power with no power compensation, P_{PC}^{WF} the new power reference from the power compensator, and P_{meas}^{WF} the obtained power with power compensation.

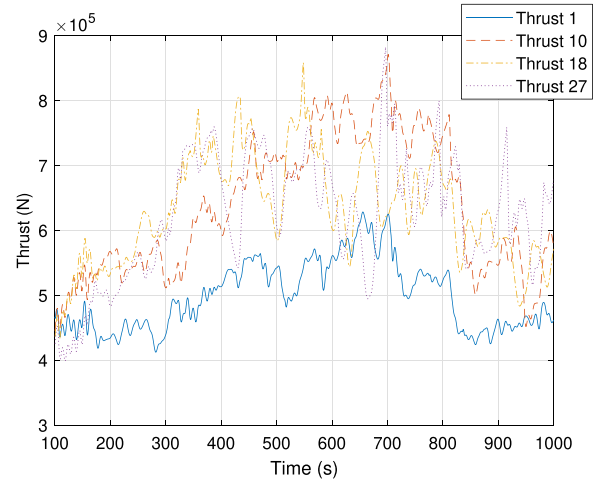


Fig. 14. Thrust forces in Scenario 2 when PC is used and TB is not used.

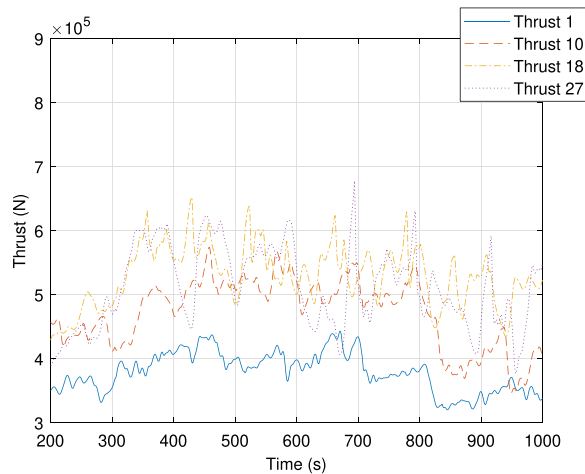


Fig. 13. Thrust forces in Scenario 2 when both PC and TB are not used.

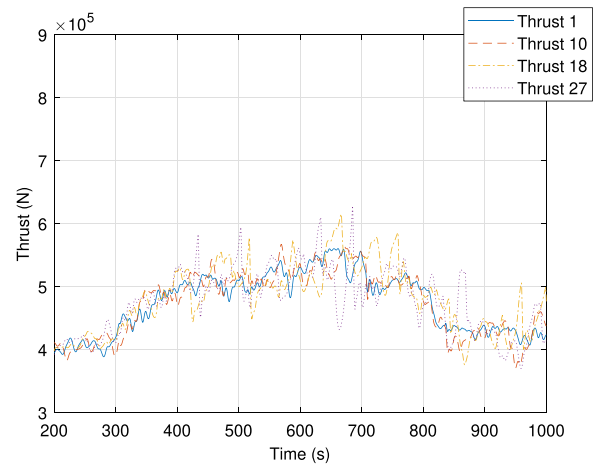


Fig. 15. Thrust forces in Scenario 2 when both PC and TB are used.

the individual power generation and demand — Fig. 11. The result is illustrated by plotting only turbines 1, 10, 18, and 27, which are ones of a four-turbine interacting set. This leads to a compromising total wind farm power generation without the PC, as seen in Fig. 12. However, as clear evidence of the benefits of the wake-loss compensator in such a scenario, not all the boosted individual power references are being matched by their power generation, but the total wind farm power with the PC still follows the desired total power.

The downside of this approach is that power booster as a simple strategy does not consider the wind turbine interactions in the dispatch of the additional power signals in the reference of each turbine (see Figs. 14 and 16). It can lead to a large variance in loads across the turbines on the farm. This variance is also seen without the PC (see Fig. 13). To convey such a downside, an additional thrust balancer is proposed and its results will be provided.

Thrust balance. The thrust balancing is designed by an additional close-loop to balance loads of unsaturated turbines while the total power reference is met by the wind farm. The result of the thrust balancer

is presented in Fig. 17 for Scenario 1, where “TB” denotes thrust balancer. The difference can be seen by comparing the loads with the case without TB in Fig. 16. As expected due to the inflow turbulence, the thrust signals keep oscillating, but their averages are balanced. This lead to aggregated structural load alleviation in the farm and a dispatch of power references that benefits the total available power [38]. For Scenario 2, the result is depicted in Fig. 15.

Load limitation. According to the decision of the turbine to be limited and its load threshold by the wind farm operator or health monitoring system, the turbine is derated using its estimated instantaneous loads as real-time feedback information. The load limitation is denoted as “LL”. The two cases were set by limiting the thrust on the turbine number eighteen (WT18), which is a waked turbine in Scenario 1 and a second downstream waked turbine in Scenario 2. In the first case, a thrust limit of 410 kN was defined, while in the second case a higher limit of 460 kN was chosen, as they are about half of the thrust variation means from previous simulations, see Figs. 18 and 19.

4.4. Quantitative results and discussions

The quantitative results are presented in three stages. All quantities are obtained after an initializing simulation time of 300 s, in which the wakes have been allowed to propagate through the farm. First, the power tracking capability is presented in Table 3. It provides a

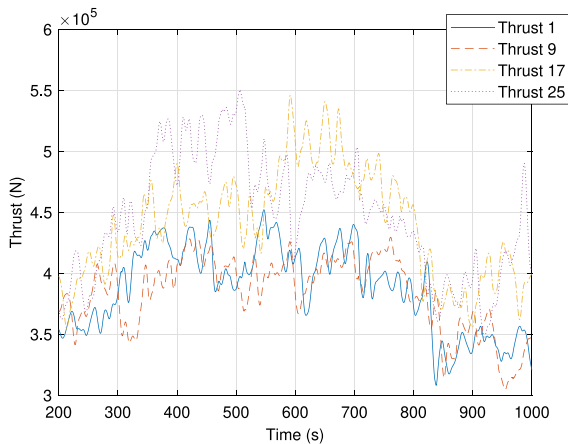


Fig. 16. Thrust forces in Scenario 1 when PC is used and TB is not used.

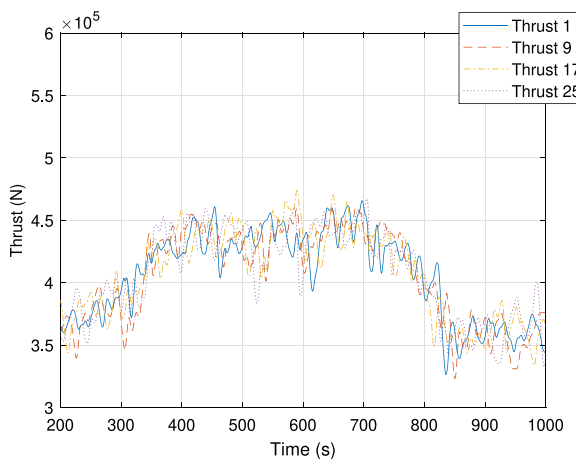


Fig. 17. Thrust forces in Scenario 1 when both PC and TB are used.

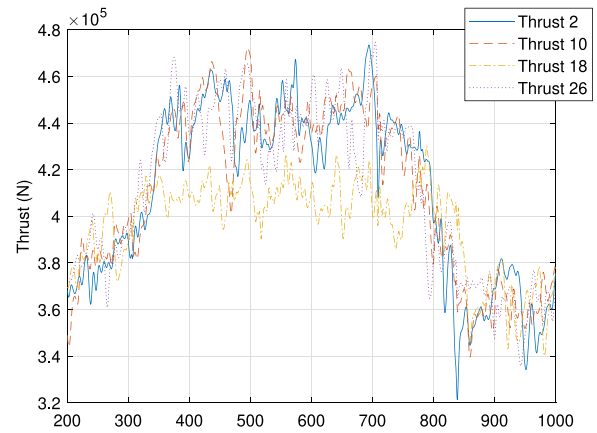


Fig. 18. Thrust forces in Scenario 1 when both PC and TB are used. In addition, LL of 410kN in the WT 18 is applied.

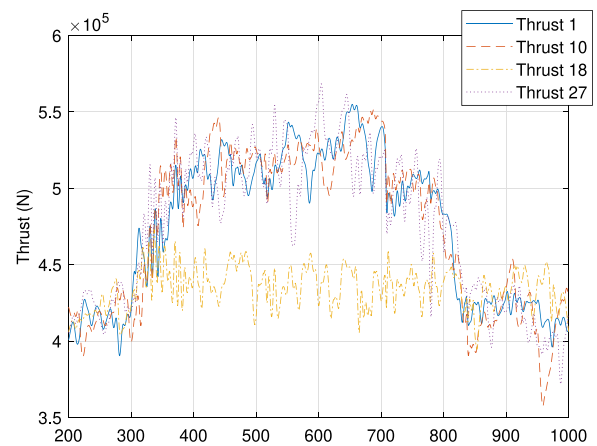


Fig. 19. Thrust forces in Scenario 2 when both PC and TB are used. In addition, LL of 450kN in WT 18 is applied.

quantitative comparison of reliability in terms of power generation from the entire farm from both scenarios, namely here as Sc1 and Sc2. The results show that the power tracking is improved with the PC based on all criteria compared to not using it. Furthermore, the power tracking is conserved or even improved by applying the TB on top of the PC. A slight improvement with the use of the LL is also noticed from the RMSEs and the MAEs, although the RMSE in Scenario 2 and the PEs increase compared with the PC and TB together.

Next, the actuation is herein evaluated because controllers can lead to premature degradation of actuation systems. For an overall wind farm evaluation, the averages of the time series of the operational

Table 3
Total power tracking criteria in the wind farm.

Scenario	PC	TB	LL	RMSE [MW]	MAE [MW]	PE [MW]
Sc1	✓			1.295	0.856	2.698
	✓	✓		0.114	0.061	0.477
	✓	✓	✓	0.081	0.042	0.468
Sc2	✓			6.044	3.802	10.765
	✓	✓		0.247	0.137	0.765
	✓	✓	✓	0.142	0.076	0.502
				0.167	0.071	1.316

* The colors in the cells go from green as the lowest value to yellow the highest value corresponding to the evaluated category. This color formatting is carried along the next tables.

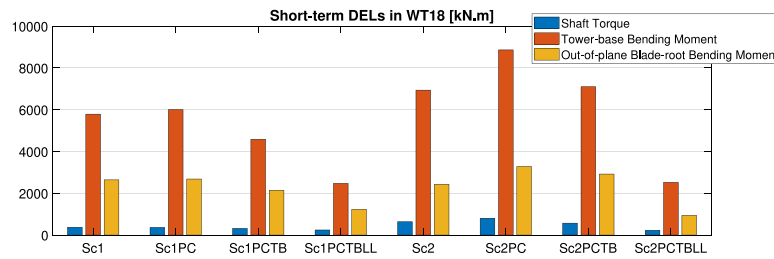


Fig. 20. Short-term damage equivalent loads for the different controllers and scenarios in WT 18.

Table 4

Statistics of the time-series average of pitch actuation and of the generator torque in the wind farm.

Scenario	PC	TB	LL	Mean [deg]	[kN m]	SD [deg]	[kN m]	Max [deg]	[kN m]	Min [deg]	[kN m]
Sc1	✓			7.6	101.9	1.5	0.1	9.7	102.1	5.5	101.6
	✓			4.6	99.5	3.2	3.4	9.4	102.4	1.2	93.2
	✓	✓		7.5	102.6	1.5	0.1	9.6	102.8	5.4	102.3
	✓	✓	✓	4.0	102.6	3.0	6.0	8.7	108.1	1.0	92.4
Sc2	✓			7.5	102.5	0.9	4.7	8.8	109.3	6.2	96.2
	✓			4.2	102.4	2.1	11.1	7.4	119.9	2.1	90.4
	✓	✓		8.3	102.7	0.8	4.4	9.4	108.4	7.1	95.8
	✓	✓	✓	5.5	102.5	1.8	10.1	8.2	118.5	3.3	89.5

Table 5

Short-term DELs of the shaft torque, tower-base bending moment, and out-of-plane blade-root bending moment [kN m].

Case	WT1	WT2	WT3	WT4	WT5	WT6	WT7	WT8
Sc1	421	3767	1525	394	4526	1975	351	4055
Sc1PC	416	3973	1654	395	4617	2021	345	4037
Sc1PCTB	395	3887	1624	366	4227	1926	340	3669
Sc1PCTBLL	311	3744	1614	328	4137	1860	269	3476
Sc2	288	3508	1487	323	3626	1629	291	2999
Sc2PC	414	5019	2132	371	5105	2234	369	4616
Sc2PCTB	345	4614	1903	332	4583	1931	319	4625
Sc2PCTBLL	336	4579	1949	312	4500	2133	308	4085

Note that the load-limiting in Sc1PCTBLL and in Sc1PCTBLL is applied in wind turbine eighteen (WT18).

parameters across the farm were computed and the statistics apply to them, as provided in Table 4. The mean of pitch actuation is reduced by applying the PC, however, the pitch and the generator torque variations are increased among turbines in the farm. This elucidates the variation in the operation of turbines due to the only use of the PC. The opposite is observed when applying the TB. The TB reduces the variance in the operation of the turbines in waked conditions. Furthermore, The LL reduces the mean of pitch actuation as a consequence of the compensation for the power losses of the load-limited turbine. However, as expected the variations increase in both pitch and generator torque due to the discrepancies in the operation of the load-limited turbine.

Finally, fatigue loads are reported in Table 5 through the short-term DEL of the torque in the rotor shaft, of the tower-base bending moment, and the out-of-plane blade root bending moment. These quantities directly address the central question of how closed-loop control considering structural loads could be beneficial for wind farm APC. For the addition of the TB on the PC, we derived the reduction of

the standard deviations across the farm of the short-term DELs of the torque in the rotor shaft, of the tower-base bending moment, and the out-of-plane blade root bending moment. The result is a reduction of 5%, 60% and 60%, respectively, in Scenario 1; and 22%, 32% and 36% in Scenario 2. This means that the damage is distributed with the addition of the TB. Applying the LL in the defined WT18, the DELs are reduced considerably in all three loads of interest – 23%, 46% and 42%, respectively, in Scenario 1; and 60%, 64% and 68% in Scenario 2 compared with the PCTB cases – while in the other turbines the DELs are held uniformly because of the TB. The DELs of WT18 from all simulations are depicted in Fig. 20. According to MLife [60] and as expected, the mechanical life of the turbines for the shaft, tower, and blades in all studied cases is considered infinity, which is not suitable for the evaluation of lifetime extension from this work. This happens because the power tracking approach (derating) experiences lower loads than the traditional operation that maximizes power extraction, which is an outstanding advantage.

5. Conclusions

Under increased wind energy penetration in the grid, APC services are essential to the reliability of power grids. An APC objective is to have the wind farm's power generation track a power reference signal generated by transmission system operators. Due to the uncertain wake dynamics, a closed-loop control solution is proposed to provide power tracking. Since dynamical wake models are generally complex, approximations are proposed such that the closed loop can be employed with a low computational cost to work in a real-time application. In addition, induced loads are considered to prevent turbines from quick degradation and to keep them safe in damaging conditions.

In this paper, we showed that wind power plants exploring APC services can provide power tracking, and reduce the loading on a farm level and specific turbines by considering additional closed loops. The application of proposed closed-loop approaches is demonstrated and evaluated in a high-fidelity simulation environment by including load examination of turbine components.

The key elements addressed in this paper are the followings: (1) wake-loss compensation, which balances the total power generated with the consumed on the grid in the presence of wake effects; (2) thrust force balancing, which balances the structural loading across the farm; (3) load-limiting control, which increases safe margins on structural-damaged turbines by limiting the instantaneous loads to user-defined ones.

Consequently, we demonstrate that power reliability is enhanced with (1). Also, damage loading is evenly spread across the turbines due to (2), which would lead to lower maintenance costs in the long term as sporadic maintenance events would be reduced. Moreover, the damage is mitigated effectively on the defined turbine by (3). The combination of such strategies could lead to a relevant cost reduction in wind energy. However, a quantitative overall cost–benefit analysis of an integrated APC for a wind farm has not yet been performed and remains the subject of ongoing and future work.

Further research and possible test campaigns are needed to implement the closed-loop controllers successfully in real wind farms. This research direction is relevant for reductions in the Levelized cost of energy (LCoE), particularly if extended as part of an overall co-optimization framework, such as by Ashuri et al. [61]. Worthwhile future avenues of investigation include time-varying wind direction and yaw control strategies like wake steering for load mitigation.

CRedit authorship contribution statement

Jean Gonzalez Silva: Conceptualization, Methodology, Simulation, Data process, Visualization, Investigation, Writing – original draft, Writing – review & editing. **Riccardo Ferrari:** Methodology, Writing – review & editing, Supervision. **Jan-Willem van Wingerden:** Methodology, Writing – review & editing, Supervision.

Declaration of competing interest

The authors declare that they have no known competing financial interests or personal relationships that could have appeared to influence the work reported in this paper.

Data availability

Data will be made available on request.

Acknowledgments

The authors would like to acknowledge the WATEREYE project (grant no. 851207). This project has received funding from the European Union Horizon 2020 research and innovation programme under the call H2020-LC-SC3-2019-RES-TwoStages.

References

- [1] Global Wind Energy Council, Global wind report 2022, 2022, URL <https://gwec.net/global-wind-report-2022/>, (Accessed: 2022-08-17).
- [2] F. Díaz-González, M. Hau, A. Sumper, O. Gomis-Bellmunt, Participation of wind power plants in system frequency control: Review of grid code requirements and control methods, *Renew. Sustain. Energy Rev.* 34 (2014) 551–564, <http://dx.doi.org/10.1016/j.rser.2014.03.040>.
- [3] M. Altin, R. Teodorescu, B. Bak-Jensen, P. Rodríguez, F. Iov, P.C. Kjær, Wind power plant control - an overview, in: 9th International Workshop on Large-Scale Integration of Wind Power Into Power Systems, Energynautics GmbH, 2010.
- [4] BEIS, Digest of UK energy statistics (DUKES) 2021, 2021, URL <https://gwec.net/global-wind-report-2022/>, (Accessed: 2022-08-17).
- [5] A.G. Isemonger, The evolving design of RTO ancillary service markets, *Energy Policy* 37 (1) (2009) 150–157, <http://dx.doi.org/10.1016/j.enpol.2008.06.033>.
- [6] E. Ela, V. Gevorgian, P.A. Fleming, Y.C. Zhang, M. Singh, E. Muljadi, A. Scholbrook, J. Aho, A. Buckspan, L.Y. Pao, V. Singhvi, A. Tuohy, P. Pourbeik, D. Brooks, N. Bhatt, Active power controls from wind power: Bridging the gaps, 2014, <http://dx.doi.org/10.2172/1117060>.
- [7] P. Fleming, J. Aho, P. Gebraad, L. Pao, Y. Zhang, Computational fluid dynamics simulation study of active power control in wind plants, in: 2016 American Control Conference (ACC), 2016, pp. 1413–1420, <http://dx.doi.org/10.1109/ACC.2016.7525115>.
- [8] J.W. van Wingerden, L. Pao, J. Aho, P. Fleming, Active power control of waked wind farms, *IFAC-PapersOnLine* 50 (1) (2017) 4484–4491, <http://dx.doi.org/10.1016/j.ifacol.2017.08.378>, 20th IFAC World Congress.
- [9] C.R. Shapiro, P. Bauweraerts, J. Meyers, C. Meneveau, D.F. Gayme, Model-based receding horizon control of wind farms for secondary frequency regulation, *Wind Energy* 20 (7) (2017) 1261–1275, <http://dx.doi.org/10.1002/we.2093>.
- [10] A.S. Ahmadyar, G. Verbič, Coordinated operation strategy of wind farms for frequency control by exploring wake interaction, *IEEE Trans. Sustain. Energy* 8 (1) (2017) 230–238, <http://dx.doi.org/10.1109/TSTE.2016.2593910>.
- [11] S. Boersma, B. Doekemeijer, S. Siniscalchi-Minna, J.W. van Wingerden, A constrained wind farm controller providing secondary frequency regulation: An LES study, *Renew. Energy* 134 (2019) 639–652, <http://dx.doi.org/10.1016/j.renene.2018.11.031>.
- [12] M. Tsili, S. Papathanassiou, A review of grid code technical requirements for wind farms, *IET Renew. Power Gener.* 3 (3) (2009) 308–332, <http://dx.doi.org/10.1049/iet-rpg.2008.0070>.
- [13] D.A. Juangarcia, I. Eguinoa, T. Knudsen, Derating a single wind farm turbine for reducing its wake and fatigue, *J. Phys. Conf. Ser.* 1037 (2018) 032039, <http://dx.doi.org/10.1088/1742-6596/1037/3/032039>.
- [14] D. van der Hoek, S. Kanev, W. Engels, Comparison of down-regulation strategies for wind farm control and their effects on fatigue loads, in: 2018 American Control Conference (ACC), 2018, pp. 3116–3121, <http://dx.doi.org/10.23919/ACC.2018.8431162>.
- [15] V. Pettas, P.W. Cheng, Down-regulation and individual blade control as lifetime extension enablers, *J. Phys. Conf. Ser.* 1102 (1) (2018) <http://dx.doi.org/10.1088/1742-6596/1102/1/012026>.
- [16] EirGrid, EirGrid grid code version 10.0, 2021, URL <https://www.eirgridgroup.com/customer-and-industry/general-customer-information/grid-code-info/>, (Accessed: 2022-08-17).
- [17] National Grid Electricity System Operator Limited, The grid code, 2021, URL <https://www.nationalgrideso.com/electricity-transmission/industry-information/codes/grid-code/code-documents>, Issue 6, Revision 13. (Accessed: 2022-08-17).
- [18] ENTSO-E, ENTSO-E network code for requirements for grid connection applicable to all generators, 2016, URL https://www.entsoe.eu/network_codes/, (Accessed: 2022-08-17).
- [19] J. Aho, P. Fleming, L.Y. Pao, Active power control of wind turbines for ancillary services: A comparison of pitch and torque control methodologies, in: American Control Conference (ACC), 2016, pp. 1407–1412, <http://dx.doi.org/10.1109/ACC.2016.7525114>.
- [20] J. Zhu, K. Ma, M. Soltani, A. Hajizadeh, Z. Chen, Comparison of loads for wind turbine down-regulation strategies, in: 2017 11th Asian Control Conference (ASCC), 2017, pp. 2784–2789, <http://dx.doi.org/10.1109/ASCC.2017.8287618>.
- [21] W.H. Lio, M. Mirzaei, G.C. Larsen, On wind turbine down-regulation control strategies and rotor speed set-point, *J. Phys. Conf. Ser.* 1037 (2018) 032040, <http://dx.doi.org/10.1088/1742-6596/1037/3/032040>.
- [22] K. Kim, H. Kim, C. Kim, I. Paek, C. Bottasso, F. Campagnolo, Design and validation of demanded power point tracking control algorithm of wind turbine, *Int. J. Precis. Eng. Manuf.-Green Technol.* 5 (2018) 387–400, <http://dx.doi.org/10.1007/s40684-018-0041-6>.
- [23] V. Spudić, C. Conte, M. Baotić, M. Morari, Cooperative distributed model predictive control for wind farms, *Optim. Control Appl. Methods* 36 (3) (2015) 333–352, <http://dx.doi.org/10.1002/oca.2136>.
- [24] D. Madjidian, Scalable minimum fatigue control of dispatchable wind farms, *Wind Energy* 19 (10) (2016) 1933–1944, <http://dx.doi.org/10.1002/we.1960>.

- [25] S. Boersma, B.M. Doekemeijer, P.M.O. Gebraad, P.A. Fleming, J. Annoni, A.K. Scholbrock, J.A. Frederik, J.W. van Wingerden, A tutorial on control-oriented modeling and control of wind farms, in: 2017 American Control Conference (ACC), 2017, pp. 1–18, <http://dx.doi.org/10.23919/ACC.2017.7962923>.
- [26] S. Kanev, F. Savenije, W. Engels, Active wake control: An approach to optimize the lifetime operation of wind farms, *Wind Energy* 21 (7) (2018) 488–501, <http://dx.doi.org/10.1002/WE.2173>.
- [27] M. Vali, V. Petrović, G. Steinfield, L. Y. Pao, M. Kühn, An active power control approach for wake-induced load alleviation in a fully developed wind farm boundary layer, *Wind Energy Sci.* 4 (1) (2019) 139–161, <http://dx.doi.org/10.5194/wes-4-139-2019>.
- [28] S. Baros, A.M. Annaswamy, Distributed optimal wind farm control for fatigue load minimization: A consensus approach, *Int. J. Electr. Power Energy Syst.* 112 (2019) 452–459, <http://dx.doi.org/10.1016/j.ijepes.2019.04.003>.
- [29] A. Stock, M. Cole, W. Leithead, L. Amos, Distributed control of wind farm power set points to minimise fatigue loads, in: 2020 American Control Conference (ACC), 2020, pp. 4843–4848, <http://dx.doi.org/10.23919/ACC45564.2020.9147732>.
- [30] I. Eguinoa, T. Göçmen, P.B. Garcia-Rosa, K. Das, V. Petrović, K. Kölle, A. Manjock, M.J. Koivisto, M. Smailes, Wind farm flow control oriented to electricity markets and grid integration: Initial perspective analysis, *Adv. Control Appl.* 3 (3) (2021) 1–28, <http://dx.doi.org/10.1002/adc2.80>.
- [31] K. Kölle, T. Göçmen, P.B. Garcia-Rosa, V. Petrović, I. Eguinoa, T.K. Vrana, Q. Long, V. Pettas, A. Anand, T.K. Barlas, N. Cutlulis, A. Manjock, J.O. Tande, R. Ruisi, E. Bossanyi, Towards integrated wind farm control: Interfacing farm flow and power plant controls, *Adv. Control Appl.* 4 (2) (2022) 1–11, <http://dx.doi.org/10.1002/adc2.105>.
- [32] P.W. Richards, D.T. Griffith, D.H. Hodges, Smart loads management for damaged offshore wind turbine blades, *Wind Eng.* 39 (4) (2015) 419–436, <http://dx.doi.org/10.1260/0309-524X.39.4.419>.
- [33] P.A. Fleming, J. Aho, A. Buckspan, E. Ela, Y. Zhang, V. Gevorgian, A. Scholbrock, L. Pao, R. Damiani, Effects of power reserve control on wind turbine structural loading, *Wind Energy* 19 (3) (2016) 453–469, <http://dx.doi.org/10.1002/we.1844>.
- [34] S.J. Price, R.B. Figueira, Corrosion protection systems and fatigue corrosion in offshore wind structures: Current status and future perspectives, *Coatings* 7 (2) (2017) <http://dx.doi.org/10.3390/coatings7020025>.
- [35] D.T. Griffith, N.C. Yoder, B. Resor, J. White, J. Paquette, Structural health and prognostics management for the enhancement of offshore wind turbine operations and maintenance strategies, *Wind Energy* 17 (11) (2014) 1737–1751, <http://dx.doi.org/10.1002/we.1665>.
- [36] J.G. Silva, D. van der Hoek, S. Mulders, R. Ferrari, J.-W. van Wingerden, A switching thrust tracking controller for load constrained wind turbines, in: 2022 American Control Conference (ACC), 2022, pp. 4230–4235, <http://dx.doi.org/10.23919/ACC53348.2022.9867888>.
- [37] Y. Liu, R. Ferrari, J.-W. van Wingerden, Load reduction for wind turbines: an output-constrained, subspace predictive repetitive control approach, *Wind Energy Sci.* 7 (2) (2022) 523–537, <http://dx.doi.org/10.5194/wes-7-523-2022>.
- [38] J.G. Silva, B. Doekemeijer, R. Ferrari, J.-W. van Wingerden, Active power control of waked wind farms: Compensation of turbine saturation and thrust force balance, in: 2021 European Control Conference (ECC), 2021, pp. 1223–1228, <http://dx.doi.org/10.23919/ECC54610.2021.9655154>.
- [39] SOWFA, 2020, URL <https://github.com/TU-Delft-DataDrivenControl/SOWFA>, (Accessed: 2022-08-17).
- [40] OpenFOAM, 2022, URL <https://openfoam.org/>, (Accessed: 2022-08-17).
- [41] OpenFAST, 2022, URL <https://github.com/OpenFAST/openfast>, (Accessed: 2022-08-17).
- [42] Y.T. Wu, F. Porté-Agel, Large-eddy simulation of wind-turbine wakes: Evaluation of turbine parametrisations, *Bound.-Lay. Meteorol.* 138 (3) (2011) 345–366, <http://dx.doi.org/10.1007/s10546-010-9569-x>.
- [43] M. Churchfield, S. Lee, P. Moriarty, L. Martínez Tossas, S. Leonardi, G. Vijayakumar, J. Bresseur, A large-eddy simulation of wind-plant aerodynamics, in: 50th AIAA Aerospace Sciences Meeting Including the New Horizons Forum and Aerospace Exposition, 2012, <http://dx.doi.org/10.2514/6.2012-537>.
- [44] M.J. Churchfield, S. Lee, J. Michalakes, P.J. Moriarty, A numerical study of the effects of atmospheric and wake turbulence on wind turbine dynamics, *J. Turbul.* 13 (2012) N14, <http://dx.doi.org/10.1080/14685248.2012.668191>.
- [45] S. Andersen, A. Madariaga, K. Merz, J. Meyers, W. Munters, C. Rodriguez, Reference wind power plant, Tech. Rep. TotalControl Deliverable D1.3, 2018, <https://orbit.dtu.dk/en/publications/reference-wind-power-plant-d103>, (Accessed: 2022-08-17).
- [46] C. Bak, R. Bitsche, A. Yde, T. Kim, M. Hansen, F. Zahle, M. Gaunaa, J. Blasques, M. Dossing, J. Wedel Heinen, T. Behrens, Description of the DTU 10 MW Reference Wind Turbine, in: European Wind Energy Conference and Exhibition (EWEC), 2013, p. 138.
- [47] C. Pilong, PJM Manual 12: Balancing Operations, 30th ed., PJM, Audubon, PA, USA, 2013.
- [48] A. Gambier, Pitch control of three bladed large wind energy converters— a review, *Energies* 14 (23) (2021) 1–24, <http://dx.doi.org/10.3390/en14238083>.
- [49] A.S. Deshpande, R.R. Peters, Wind turbine controller design considerations for improved wind farm level curtailment tracking, in: 2012 IEEE Power and Energy Society General Meeting, 2012, pp. 1–6, <http://dx.doi.org/10.1109/PESGM.2012.6343975>.
- [50] NREL, ROSCO. Version 2.3.0, 2021, URL <https://github.com/NREL/rosc0>, (Accessed: 2022-08-17).
- [51] L.Y. Pao, K.E. Johnson, A tutorial on the dynamics and control of wind turbines and wind farms, in: 2009 American Control Conference, 2009, pp. 2076–2089, <http://dx.doi.org/10.1109/ACC.2009.5160195>.
- [52] J. Jonkman, S. Butterfield, W. Musial, G. Scott, Definition of a 5MW reference wind turbine for offshore system development, *Natl. Renew. Energy Lab. (NREL)* (2009) <http://dx.doi.org/10.2172/947422>.
- [53] S.P. Mulders, M.B. Zaaier, R. Bos, J.W. van Wingerden, Wind turbine control: open-source software for control education, standardization and compilation, *J. Phys. Conf. Ser.* 1452 (2020) 012010, <http://dx.doi.org/10.1088/1742-6596/1452/1/012010>.
- [54] J.G. Silva, B.M. Doekemeijer, R. Ferrari, J.-W. van Wingerden, Active power control of wind farms: an instantaneous approach on waked conditions, *J. Phys. Conf. Ser.* 2265 (2) (2022) 022056, <http://dx.doi.org/10.1088/1742-6596/2265/2/022056>.
- [55] M.N. Soltani, T. Knudsen, M. Svenstrup, R. Wisniewski, P. Brath, R. Ortega, K. Johnson, Estimation of rotor effective wind speed: A comparison, *IEEE Trans. Control Syst. Technol.* 21 (4) (2013) 1155–1167, <http://dx.doi.org/10.1109/TCST.2013.2260751>.
- [56] Y. Liu, A.K. Pamosuryo, R.M.G. Ferrari, J.-W. van Wingerden, The immersion and invariance wind speed estimator revisited and new results, *IEEE Control Syst. Lett.* 6 (2022) 361–366, <http://dx.doi.org/10.1109/LCSYS.2021.3076040>.
- [57] A. May, D. McMillan, S. Thöns, Economic analysis of condition monitoring systems for offshore wind turbine sub-systems, *IET Renew. Power Gener.* 9 (8) (2015) 900–907, <http://dx.doi.org/10.1049/iet-rpg.2015.0019>.
- [58] Y. Liu, R. Ferrari, P. Wu, X. Jiang, S. Li, J.-W. van Wingerden, Fault diagnosis of the 10MW floating offshore wind turbine benchmark: A mixed model and signal-based approach, *Renew. Energy* 164 (2021) 391–406, <http://dx.doi.org/10.1016/j.renene.2020.06.130>.
- [59] S. Laghrouche, F. Plestan, A. Glumineau, Higher order sliding mode control based on integral sliding mode, *Automatica* 43 (3) (2007) 531–537, <http://dx.doi.org/10.1016/j.automatica.2006.09.017>.
- [60] MLife, 2012, URL <https://www.nrel.gov/wind/nwtc/mlife.html>, (Accessed: 2022-08-17).
- [61] T. Ashuri, M.B. Zaaier, J.R. Martins, G.J. van Bussel, G.A. van Kuik, Multidisciplinary design optimization of offshore wind turbines for minimum leveled cost of energy, *Renew. Energy* 68 (2014) 893–905, <http://dx.doi.org/10.1016/j.renene.2014.02.045>.